RSC Advances

ROYAL SOCIETY OF CHEMISTRY

www.rsc.org/advances

Graphene-based three-dimensional hierarchical sandwich-type architecture for high performance supercapacitors

Yufei Zhang[1,3], Mingze Ma[1], Jun Yang[1], Wei Huang[1,2*], Xiaochen Dong[1,2,4*]

[1] Jiangsu-Singapore Joint Research Center for Organic/Bio-Electronics & Information Displays and Institute of Advanced Materials (IAM), Nanjing Tech University, 30 South Puzhu Road, Nanjing 211816, China

[2] Key Laboratory for Organic Electronics & Information Displays (KLOEID), Nanjing Tech University, 30 South Puzhu Road, Nanjing 211816, China

[3] School of Chemistry and Chemical Engineering, Inner Mongolia University, Huhhot 010021, China

[4] State Key Laboratory of Materials-Oriented Chemical Engineering, Nanjing Tech University, 30 South Puzhu Road, Nanjing 211816, China

iamwhuang@njut.edu.cn (W Huang), iamxcdong@njut.edu.cn (XC Dong)

Abstract

A facile two-step method is developed for large-scale preparation of graphene-based three-dimensional hierarchical sandwich-type architecture (graphene/carbon nanotubes (CNTs)/Mn_2O_3) for high performance supercapacitor. The synthesis involves a chemical vapor deposition (CVD) method to fabricate sponge-like three-dimensional (3D) graphene/CNTs and a electrodeposition process to deposit Mn_2O_3 nano-sheets on the surface of 3D graphene/CNTs. With the novel sandwich-type composite as electrode, the measurements indicate the synergy effects of Mn_2O_3 and 3D carbonous materials make the electrode present a high specific capacitance. The composite electrode also presents a high reversible capacity, excellent cycle performance and rate capability. It could be

concluded that the composite of Mn_2O_3 with 3D graphene/CNTs displays excellent synergy effects of transition-metal oxide and carbonous materials. This work also inspires deep research for the application of 3D graphene-based composites for high performance supercapacitors.

1. Introduction

With the increasing concerns over energy supplies, there has been an urgent demand for seeking cleaner energy storage devices. During the past few years, research into supercapacitors has experienced a massive growth due to its high specific capacitance, pulse power capabilities, and long cycle life.[1-5] At present, researchers mainly focus on the highly porous carbon materials because the high surface area of porous carbon electrodes can aggrandize the interaction between the electrolyte ions and the electrode.[6,7] In order to develop novel materials capable of accumulating more charge per unit area, several carbon based nanomaterials, such as carbon nanotubes, carbon fibers and graphene have been explored as the electrode materials in supercapacitors.[8-11] Among these, graphene, a two-dimensional monolayer of sp^2 hybridized carbon atoms, has attracted tremendous interests in recent years due to its extraordinary electrical properties, unusual mechanical strength, and ultra-large specific surface area.[12-14] Compared to traditional 3D graphene foam assembled by graphene oxide nano-sheets, the 3D graphene foam, synthesized by CVD with nickel foam as substrate, presents several peculiar advantages.[15-17] First, the defect-free and freement of inter-sheet junction-resistance of seamlessly continuous 3D graphene provide the CVD-grown 3D graphene high conductivity. Second, the 3D graphene foam exhibits an extremely high specific surface area due to the overcoming of the strong π-π interaction between graphene sheets. Thus,

the porous 3D CVD-grown graphene foam is suitable to make functional composites by surface modification with nano-particles or other functional materials.[18] By the combination of graphene and carbon nanotube, it can overcome the shortage of limited effective surface area due to their planar (2D) geometry. Also, the roughness surface of graphene/CNTs is useful for the fabrication of graphene based composite. Various transition-metal oxides have been widely explored for the electrodes of supercapacitors as well.[19-22] Among them, manganese oxides (MnO, MnO_2, Mn_2O_3, etc) are generally considered to be one of the most promising transition metal oxides for the next generation of supercapacitors because of its high theoretical capacity, non-toxicity, low cost, great flexibility in structures and morphology and natural abundance.[23,24] It is reported that the theoretical electric capacity of manganese oxides can reach 1370 F/g.[25] However, its bad stability and low electrical conductivity led to the difficulties in practical application.[26-28] Researches have shown that manganese oxides can obtain better performance by modified with carbonaceous materials which have good cycle stability.[29-33]

With the aim of developing a supercapacitor with high specific capacitance and excellent cycle stability, we synthesized 3D graphene/CNTs by CVD method firstly. Then, Mn_2O_3 nano-sheets were coated on its surface using electrodeposition to obtain graphene-based 3D hierarchical sandwich-type architecture composites. The electrochemical measurements indicate that the composite electrodes can achieve high specific capacitance and exhibit good cycle stability owing to the synergistic effect of 3D graphene, carbon nanotube and Mn_2O_3. Hence, the sandwich-type composites provide a direction toward solving the potential problem and are promising for the next generation high-performance electrochemical electrodes.

2.Results and Discussion

2.1. Morphology and Structure Analysis

The morphology and structure of 3D graphene/CNTs/Mn_2O_3 composite were examined by scanning electron microscopy (SEM) and transmission electron microscopy (TEM), respectively, as shown in Figure 1. The as-prepared graphene foam is monolithic with good mechanical stability and is easily handled (Figure 1a). An interconnected 3D network structure can be clearly observed in Figure 1b. The graphene foam exhibits a porous structure with the pore size of 100-300 μm and its skeleton is seamlessly continuous. This structure is useful for the enhancement of its conductivity as the porous structure increase the inter reaction of the electrolyte and the composite electrode. At higher magnification, it indicates the surface of graphene foam is micrometer scale smooth with the similar topographic domains of nickel substrate, as shown in Figure 1c. After the formation of graphene/CNTs, it can be seen that the CNTs attached on the surface of 3D graphene skeleton and exhibit a dense network structure with the diameter of 100-150nm (Figure 1d). The right insert shows the TEM image of the carbon nanotubes, which further confirm the formation of carbon nanotubes with hollow structure. From the Figure 1e, it can be seen that the skeleton of graphene/CNTs/Mn_2O_3 composite is fully and uniformly covered by Mn_2O_3 nano-sheets. The high-resolution SEM image further shows that the Mn_2O_3 nano-sheets exhibits flower-like nano-structure (Figure 1f). The unique nanostructure enlarge the surface area of Mn_2O_3, which is useful for the improvement of its capacitance performance.

The Raman spectra were also conducted to measure the structure of graphene, graphene/CNTs and the graphene/CNTs/Mn_2O_3 composite, as shown in Figure 2a. 3D

graphene shows two distinct peaks at 1575 cm^{-1} and 2740 cm^{-1}, which are attributed to the G and 2D bands of graphene sheet, respectively.[34] As revealed by the integrated intensity ratio of G and 2D bands (I_G/I_{2D}) in the Raman spectrum, the 3D graphene consists of single- and few-layer domains.[35] It is worth mentioning that the D band (~1350 cm^{-1}) cannot be discerned on the 3D graphene spectrum, suggesting the high quality of the obtained graphene.[36] In comparison with bare graphene, the Raman spectrum of the 3D graphene/CNTs has characteristic D, G and 2D peaks of multi-walled carbon nanotubes. After the formation of graphene/CNTs/Mn_2O_3 composite, its Raman spectrum not only present the characteristic D, G and 2D peaks of graphene and CNTs, but also exhibits the unique peaks of Mn_2O_3. The peaks observed around 600 cm^{-1} are ascribed to the characteristic modes of crystalline Mn-O lattice vibrations.[37]

Figure 2b shows the XRD spectra of graphene/CNTs and graphene/CNTs/Mn_2O_3 composite, respectively. The peak observed around 25° is the characteristic peak of carbon. The graphene/CNTs/Mn_2O_3 composite shows strong diffraction peaks, which are well indexed to the (211), (222) and (400) lattice planes of Mn_2O_3 structure (JCPDS card no.89-2809). The result shows that no impurity phase exists in the graphene/CNTs/Mn_2O_3 composite. It also confirms that graphene/CNTs/Mn_2O_3 composite still maintains graphene/CNTs structure after the electrodeposition of Mn_2O_3.

2.2. Electrochemical Testing

The electrochemical performance of graphene/CNTs and graphene/CNTs/Mn_2O_3 composite electrode were evaluated by cyclic voltammetry (CV) and galvanostatic charge/discharge measurement, respectively. It is well known that CV is an ideal technique for characterizing the capacitive behavior. As a material for supercapacitor,

characteristics such as a large magnitude of current and a rectangular type of voltammogram is ideal. Figure 3a presents the CV curves over a voltage range from 0 to 0.8 V of the graphene/CNTs and 3000s electrodeposited graphene/CNTs/Mn_2O_3 composite electrode measured at a scan rate of 20 mV/s. It can be seen that the responses of both graphene/CNTs and graphene/CNTs/Mn_2O_3 electrodes are very close to ideal electrochemical double layer behavior because no polarization was showed. Hahm *et al*. has analyzed this behavior indicated the electrolyte effectively used the electrode material due to the well-spaced nanostructured geometry.[7] Obviously, the area surrounded by the CV curve is dramatically enhanced by the introduction of Mn_2O_3 onto graphene/CNTs. As known, the area of each closed CV curve suggests its specific capacitance, the increase in area of the CV curve for the graphene/CNTs/Mn_2O_3 composite compared to the graphene/CNTs indicates the sandwich type architecture has a large enhanced capacitance. The high electronic conductivities of graphene/CNTs materials do not necessarily translate into a high capacitance because the capacitance also depends on other important parameters, such as the pore size, the degree of functionalization, and the accessibility of electrolyte.[38] So after depositing Mn_2O_3, the chemical performance of the composite is greatly improved by both the pseudocapacitive behavior of Mn_2O_3 and the electrical double layer capacitive behavior of graphene/CNTs.

Furthermore, as shown in the Figure 3a, the redox peak current from the graphene/CNTs/Mn_2O_3 composite electrode is much larger than that from the graphene/CNTs electrode. Comparing graphene/CNTs/Mn_2O_3 electrodes prepared by different electrodeposition time at scan rate of 20mV/s, it is evident that the CV curve is enhanced by prolonging the electrodeposition time, as shown in Figure 3b. Increasing the

scan rate also leads to further increase of the redox peaks current (Figure 3c), confirming the pseudocapacitive behavior of the composite electrode and a surface-confined electrochemical process. Further increase the scan rate to 1, 2, 5 and 10V/s within 0.0 0.8 V voltage window, the electrode still present the rectangular shape even at a high scan rate of 10 V/s, indicating the electrode processes the characteristic of ideal electrochemical double layer capacitive behavior even at such high areal density. This feature is contributed from synergistic effects by the combined 3D graphene, CNTs and Mn_2O_3. Therefore, it can be concluded that ultrahigh power can be obtained from this kind of device.[39]

Figure 4a depicts the galvanostatic charge-discharge curves of the graphene/CNTs/Mn_2O_3 sandwich electrode prepared by electrodeposition for 3000s at different current densities. The specific capacitance could be calculated from the following equation:[40]

$$C=I\times\Delta t/(m\times\Delta V) \quad (1)$$

Where C is the specific capacitance of the electrode between 0 and 0.5V (F g^{-1}), I refers to the current density used for the charge-discharge measurements (A), t refers to the discharging time (s), ΔV is the potential window for the cycling test, and m denotes the weight of the graphene/CNTs/Mn_2O_3 electrode. According to the equation, the discharge areal capacitance of the graphene/CNTs/Mn_2O_3 composite electrode at 100, 250, 400 and 500 mA/g is 370, 320, 301 and 280.9 F/g, respectively. It is larger than that of pure graphene and graphene/CNTs.

Figure 4b shows effect of electrodeposition time on the specific capacitance of graphene/CNTs/Mn_2O_3 at various discharge current densities calculated from the formula

(1). It can be seen that the specific capacitance increased with prolonging the deposition time. These could be attribute to the fact that the mass of the Mn_2O_3 is unsurprisingly increased as the deposition time extended. However, continue extending the deposition time over the optimal range, the morphology of the sample could be changed and lead to the reduction of the specific surface area of Mn_2O_3 exposed to electrolyte ions, which results in the decrease of the specific capacitance.[41] Therefore, the optimal composite is electrodeposited for 3000s. TGA analysis indicates that the weight percentage of Mn_2O_3 in the electrodes deposited 1000s, 2000s and 3000s is about 36 %, 66 % and 72 %, respectively.

More importantly, the 3000s electrodeposited graphene/CNTs/Mn_2O_3 sandwich type porous composite electrode has a good columbic efficiency for each cycle of charge and discharge, which indicates a good electrochemical stability (Figure 4c). Even after many times of charge-discharge cycle(>1000 cycles), the charge-discharge curves remain symmetric. These may be attributed to the synergistic effect of 3D graphene, CNTs and Mn_2O_3. Graphene and CNTs, with good conductivity, can support the nano-scaled Mn_2O_3 and improve the contact between the active materials and the electrolyte. It also provide electronically conductive channels for electrons to enlarge the interface between the composites and electrolyte. Furthermore, CNTs can change the roughness of the surface, which makes Mn_2O_3 tightly attached on the electrode and improves the stability of the electrodes.

Figure 4d shows evolution of the specific capacitance versus the cycle number at a current density of 1A/g. It can be seen that the specific capacitance of the 3000 s deposited composite electrode can be further enhanced at the initial cycles and stays

stable afterwards. Such activation process may result from the more complete intercalation and de-intercalation of electrochemical species after several initial cycles. After that, the specific capacitance is very stable. These results reveal that the high specific capacitance, remarkable rate capability and excellent cycle stability for supercapacitors of the graphene/CNTs/Mn_2O_3 composite electrode. These remarkable electrochemical performance could certainly be attributed to two reasons. First, the conductive graphene and CNTs could enhance the specific capacitances of Mn_2O_3 through improving their electrical conductivity. Second, the flower-like Mn_2O_3 has large surface area, which increase the pseudocapacitive reactions between manganese oxides and Na^+ occurred on their surface.[42]

To further evaluate the electrochemical behaviors of the graphene/CNTs/Mn_2O_3 electrode prepared by electrodeposition for 400, 1000, 2000 and 3000 s, respectively, the Nyquist plots of different electrodes were presented in Figure 5. The impedance curves were carried out in a frequency of 1 Hz to 10 kHz. It can be seen that each sample exhibits a straight oblique line in the low-frequency range. The more vertical curve suggests the better capacitive behavior of supercapacitor assembly.[43] The 3000 s deposited sample shows the best vertical curve compared to the others, suggesting the best capacitive behavior. This may be attributed to the highly reversible redox reactions associated with Mn_2O_3 nanoparticles along with better electrical conductivity provided by the graphene and CNTs.[44]

3. Conclusions

In summary, graphene-based 3D hierarchical sandwich-type architecture with high specific capacitance were fabricated with a facile chemical vapor deposition and

electrodeposition procedure. Serving as a free-standing electrode for supercapacitor, 3D graphene along with the electrodeposited Mn_2O_3 provided the sandwich type electrode a porous structure, which makes electrolyte fully access to Mn_2O_3 easily and improves the specific performances of graphene/CNTs/Mn_2O_3 electrodes dramatically. The electrochemical measurement indicates that the sandwich-type composite electrode exhibits excellent electrochemical activity even at the scan rate of 10 V/s. The excellent cycle stability and supercapacitor performance attributed to its large active surface area and rapid charge transfer rate, which allowed the electrolyte easily transfer during the rapid charge-discharge process. These results suggest that porous structure enabled by the synergistic effects of carbonous materials and metal oxide may offer an promise for the development of high-performance supercapactiors.

4.Experimental Section

Synthesis of 3D graphene/CNTs

The 3D graphene/CNTs were synthesized by a two-step CVD method. Firstly, the 3D graphene foam was synthesized by CVD using nickel foam (thickness 1.0 mm) as the substrate and ethanol as the precursor under atmospheric pressure.[45,46] After 20 min growth, the obtained graphene/Ni foams were immersed into $NiCl_2$ solution (0.1 mM) containing 7% (w/w) polyethylene glycol for 3 min and dried in air. Subsequently, the graphene/nickel foams were loaded into a quartz tube for the CVD growth of carbon nanotubes at 750 □ for 40 min, still using ethanol as the precursor. Finally, the Ni substrates were etched away using 3 M HCl at 80 □ overnight to leave the free-standing 3D graphene/CNTs.

Synthesis of graphene/CNTs/Mn_2O_3 composites

The sandwich-type porous graphene/CNTs/Mn_2O_3 sandwich electrode were prepared by a following electrochemical deposition step after obtaining the 3D graphene/CNTs composites.[47,48] The electrodeposition was performed using an electrochemical workstation (CHI 760D, CH instrument Inc, China) with graphene/CNTs as working electrode, Pt foil as counter electrode and Ag/AgCl as reference electrode. A constant potential of 1.0 V was applied in an aqueous solution of 0.01 mol/L manganese acetate for 400, 1000, 2000 and 3000s, respectively. The products was then washed with double-distilled water several times and dried by nitrogen atmosphere. Finally, the sample was calcinated at 200□ in air for 3 h to obtain the highly crystalline Mn_2O_3 on the surface of graphene/CNTs.

Materials Characterization

3D graphene/CNTs was observed with scanning electron microscopy (SEM) (JOEL JSM-6700F) and transmission electron microscopy (TEM) (JEOL JEM-1400F). The Raman spectra (excited at 488 nm) were obtained by a Confocal Raman microscope (CRM200, WITec). The X-ray diffraction (XRD) was carried out on a Bruker D8 Advanced Diffractometer using Cu Kα radiation. Thermal gravimetric analysis (TGA) was carried out with simultaneous thermal analyzer (STA449F3).

Electrochemical Tests

All electrochemical measurements were carried out using an electrochemical workstation (CHI 760D, CH instrument Inc, China). A conventional three-electrode system was employed with 3D graphene/CNTs/Mn_2O_3 composite electrode as the working electrode, Ag/AgCl electrode as the reference, and platinum plate as the counter electrode. 1.0 M Na_2SO_4 was used as electrolyte for all the electrochemical tests.

Acknowledgements

The authors gratefully acknowledge the financial support by Jiangsu Provincial Founds for Distinguished Young Scholars (SBK201310284), the NNSF of China (21275076, 61328401) , the Key Project of Chinese Ministry of Education (212058), Research Fund for the Doctoral Program of Higher Education of China (20123223110008), the opening project of the State Key Laboratory of Materials-Oriented Chemical Engineering in Nanjing Tech University (KL12-04).

References

[1] B. E. Conway, *J. Electrochem. Soc.* **1991**, *138*, 1539.

[2] M. Winter, R. J. Brodd, *Chem. Rev*. **2004**, *104*, 4245.

[3] H. Wang, H. S. Casalongue, Y. Liang, H. Dai, *J. Am. Chem. Soc.* **2010**, *132*, 7472.

[4] J. R. Miller, P. Simon, *Science.* **2008**, *321*, 651.

[5] P. Simon, Y. Gogotsi, *Nat. Mater*. **2008**, *7*, 845.

[6] H. J. In, S. Kumar, Y. Shao-Horn, G. Barbastathis, *Appl. Phys. Lett*. **2006**, *88*, 083104.

[7] M. G. Hahm, A. L. M. Reddy, D. P. Cole, M. Rivera, J. A. Vento, J. Nam, H. Y. Jung, Y. L. Kim, *et al*. *Nano Lett*. **2012**, *12*, 5616.

[8] X. C. Dong, G. C. Xing, M. B. Chan-Park, W. H. Shi, N. Xiao, J. Wang, Q. Y. Yan, T. C. Sum, W. Huang, P. Chen, *Carbon.* **2011**, *49*, 5071.

[9] A. L. M. Reddy, S. Ramaprabhu, *J. Phys. Chem. C.* **2007**, *111*, 16138.

[10] D. N. Futaba, K. Hata, T. Yamada, T. Hiraoka, Y. Hayamizu, Y. Kakudate ,O. Tanaike, H. Hatori, M. Yumura, S. Iijima. *Nat. Mater.* **2006**, *5*, 987.

[11] S. Park, K. Lian, Y. Gogotsi, *J. Electrochem. Soc.* **2009**, *156*, 921.

[12] A. K. Geim, K. S. Novoselov, *Nat. Mater.* **2007**, *6*, 183.

[13] G. Eda, M. Chhowalla, *Adv. Mater.* **2010**, *22*, 2392.

[14] Y. W. Zhu, S. Murali, W. W. Cai, X. S. Li, J. W. Suk, J. R. Potts, R. S. Ruoff, *Adv. Mater.* **2010**, *22*, 3906.

[15] Z. P. Chen, W. C. Ren, L. B. Gao, B. L. Liu, S. F. Pei and H. M. Cheng, *Nat. Mater.* **2011**, *10*, 424.

[16] X. C. Dong, C. Y. Su, W. J. Zhang, J. W. Zhao, Q. D. Ling, W. Huang, P. Chen and L. J. Li, *Phys. Chem. Chem. Phys.* **2010**, *12*, 2164

[17] S. Agarwal, X. Zhou, F. Ye, Q. He, G. C. Chen, J. Soo, F. Boey, H. Zhang, P. Chen, *Langmuir.* **2010**, *26*, 2244.

[18] X. Huang, X. Y. Qi, F. Boey and H. Zhang, *Chem. Soc. Rev.* **2012**, *41*, 666.

[19] R. R. Bi, X. L. Wu, F. F. Cao, L. Y. Jiang, Y. G. Guo, L. J. Wan, *J. Phys. Chem. C.* **2010**, *114*, 2448.

[20] Y. Shan, L. Gao, *Mater. Chem. Phys*. **2007**, *103*, 206.

[21] L. Yuan, X. H. Lu, X. Xiao, T. Zhai, J. Dai, F. Zhang, B. Hu, X. Wang, L. Gong, J. Chen, *et al. ACS Nano.* **2011**, *6*, 656.

[22] S. Chen, J. W. Zhu, X. D. Wu, Q. F. Han, X. Wang, *ACS Nano.* **2009**, *4*, 2822.

[23] G. Yu, L. Hu, M. Vosgueritchian, H. Wang, X. Xie, J. R. McDonough, X. Cui, Y. Cui, Z. Bao, *Nano Lett.* **2011**, *11*, 2905.

[24] A. E. Fischer, K. A. Pettigrew, D. R. Rolison, R. M. Stroud, J. W. Long, *Nano Lett*. **2007**, *7*, 281.

[25] S. H. Li, Q. H. Liu, L. Qi, *Chin J Anal Chem*, **2012**, *40(3)*,339.

[26] L. Wei, C. Li, H. Chu, Y. Li, *Dalton Trans.* **2011**, *40*, 2332.

[27] W. Wei, X. Cui, W. Chen, D. G. Ivey, *Chem. Soc. Rev.* **2011**, *40*, 1697.

[28] Z. Li, Y. Mi, X. Liu, S. Liu, S. Yang, J. Wang, *J. Mater. Chem.* **2011**, *21*, 14706.

[29] L. Wang, D. L.Wang, *Electrochimica Acta.* **2011,** *56,*- 5010.

[30] J. H. Kim, K. H. Lee, L. J. Overzet, G. S. Lee, *Nano Lett.* **2011**, *11*, 2611.

[31] L. L. Zhang, X. Zhao, M. D. Stoller, Y. Zhu, H. Ji, S. Murali, Y. Wu, S. Perales, B. Clevenger, R. S. Ruoff, *Nano Lett*. **2012**, *12*, 1806.

[32] S. W. Lee, J. Kim, S. Chen, P. T. Hammond, Y. Shao-Horn, *ACS Nano.* **2010**, *4*, 3889.

[33] J. Liu, J. Essner, J. Li, *Chem. Mater.* **2010**, *22*, 5022.

[34] X. C. Dong, Y. M. Shi, Y. Zhao, D. M. Chen, J. Ye, Y. G. Yao, F. Gao, Z. H. Ni, T. Yu, Z. X. Shen, *et al.* Phys. *Rev. Lett.* **2009**, *102*, 135501.

[35] Z. Chen, W. Ren, L. Gao, B. Liu, S. Pei, H. M. Cheng, *Nat. Mater.* **2011**, *10*, 424.

[36] X. C. Dong, D. L. Fu, W. J. Fang, Y. M. Shi, P. Chen, L. J. Li, *Small.* **2009**, *5*, 1422.

[37] L. Mao, K. Zhang, H. S. O. Chan, J. S. Wu, *J. Mater. Chem*. **2012**, *22*, 1845.

[38] Z. D. Huang, B. Zhang, R. Liang, Q. B. Zheng, S. W. Oh, X. Y. Lin, N. Yousefi, J. K. Kim, *Carbon.* **2012**, *50*, 4239.

[39] D. Pech, M. Brunet, H. Durou, P. H. Huang, V. Mochalin, Y. Gogotsi, P. L. Taberna, P. Simon, *Nat. Nanotechnol*. **2010**, *5*, 651.

[40] C. G. Liu, Z. Yu, D. Neff, A. Zhamu, B. Z. Jang, *Nano Lett*. **2010**, *10,* 4863.

[41] H. C. Gao, F. Xiao, C. B.Ching, and H. W. Duan, *ACS Appl. Mater. Interfaces,* **2012**, *4*, 2801

[42] J. Yan, Z. Fan, T. Wei, W. Qian, M. Zhang, F. Wei, *Carbon*. **2010**, *48*, 3825.

[43] M. D. Stoller, S. Park, Y. Zhu, J. An, R. S. Ruoff, *Nano Lett*. **2008**, *8*, 3498.

[44] A. K. Mishra, S. Ramaprabhu, *J. Phys. Chem. C.* **2011**, *115*, 14006.

[45] M. W. Xu, D. D. Zhao, S. J. Bao, H. L. Li, J. *Solid State Electrochem.* **2007**, *11,* 1101.

[46] X. C. Dong, B. Li, A. Wei, X. H. Cao, M. Park, H. Zhang, L. J. Li, W. Huang, P. Chen, *Carbon.* **2011**, *49*, 2944.

[47] P. Si, X. C. Dong, P. Chen, D. H. Kim, *J. Mater. Chem. B.* **2013**, *1*, 110.

[48] X. C. Dong, Y. W. Ma, G. Y. Zhu, Y. X. Huang, J. Wang, M. B. Chan-Park, L. H. Wang, W. Huang, P. Chen, *J. Mater. Chem.* **2012***, 22,* 17044.

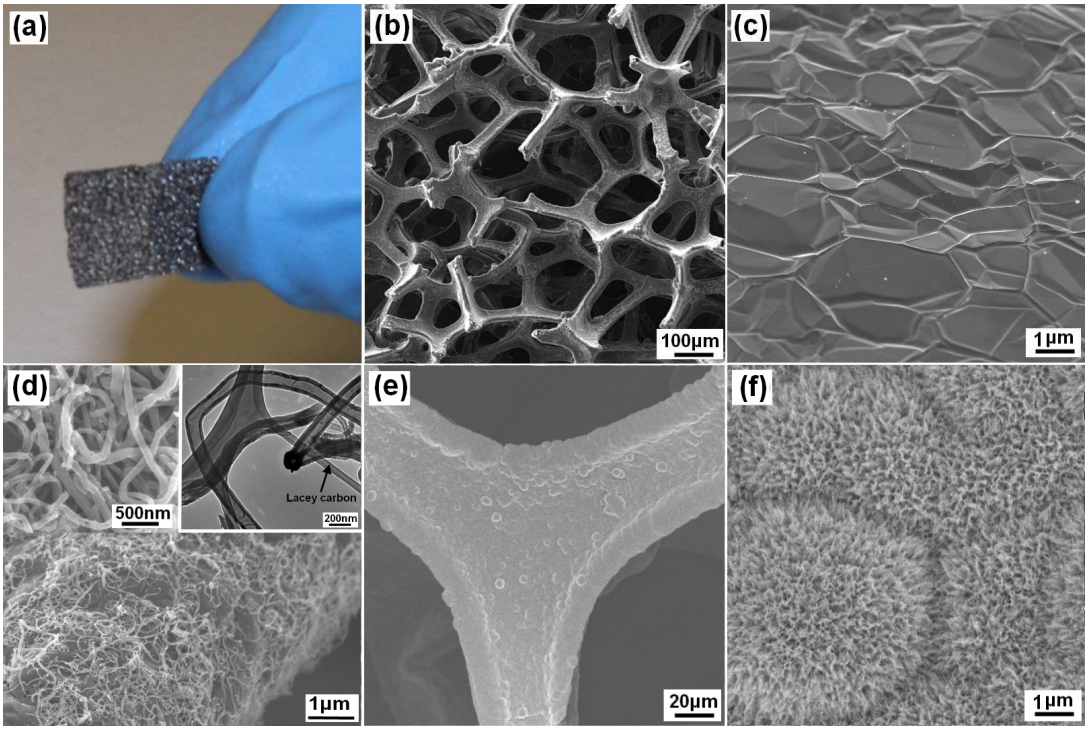

Figure 1. (a) Photograph of 3D graphene foam. (b, c) SEM images of 3D graphene foam at low- and high-magnification, respectively. (d) SEM image of 3D graphene/CNTs. The left inset shows the magnification SEM image of 3D graphene/CNTs foam, the right inset shows the TEM image of CNTs on 3D graphene. (e, f) Low- and high-magnification SEM images of Mn_2O_3 deposited for 1000s on the surface of graphene/CNTs.

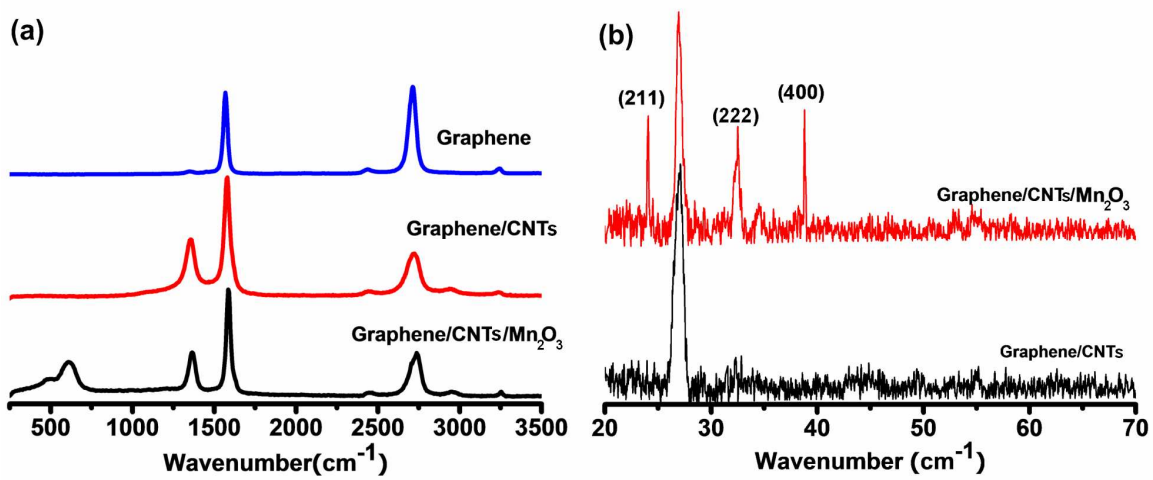

Figure 2. (a) Raman spectra of graphene, graphene/CNTs and graphene/CNTs/Mn_2O_3. (b) XRD patterns of graphene/CNTs and graphene/CNTs/Mn_2O_3

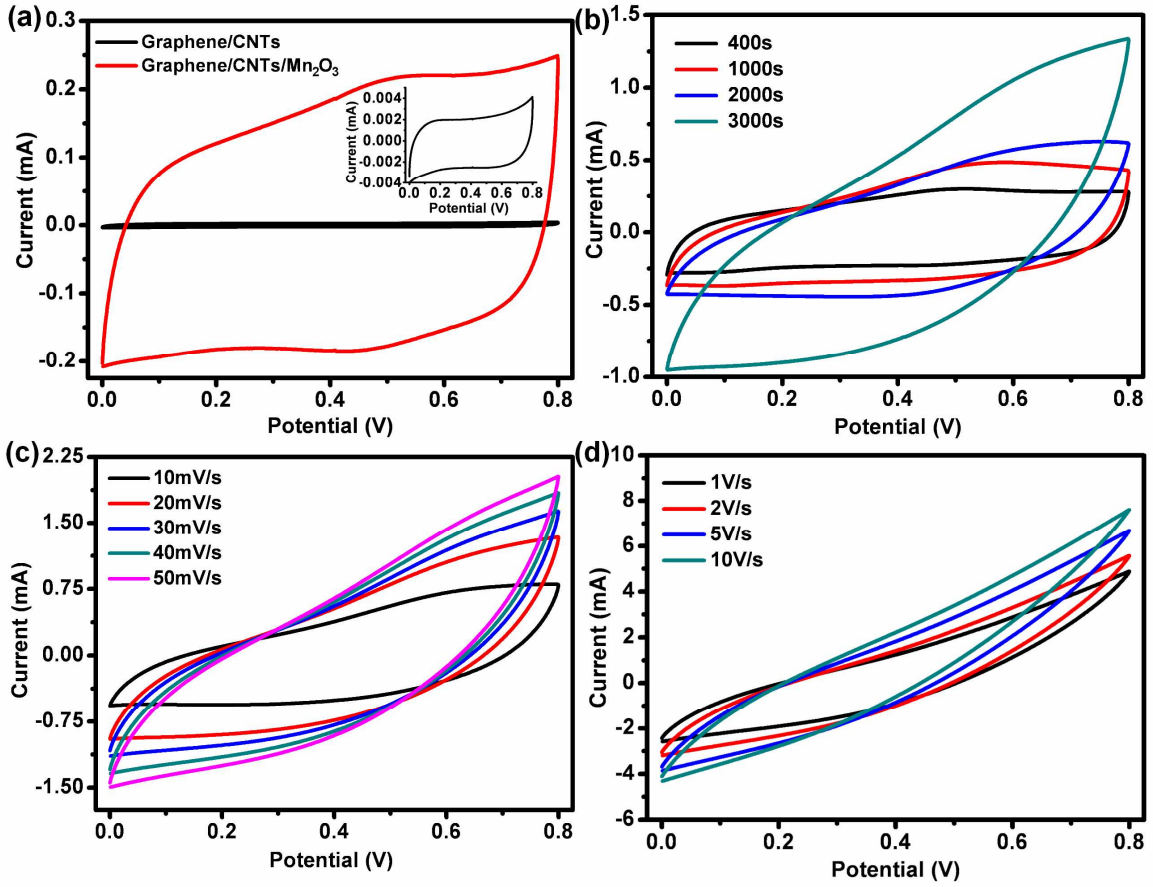

Figure 3. (a) CV curves of the graphene/CNTs and electrocdeposited 1000s graphene/CNTs/Mn_2O_3 sandwich-type electrode at a scan rate of 20 mV/s. (b) CV curves of the graphene/CNTs/Mn_2O_3 composite electrodes prepared by different electrodeposition time at scan rate of 20 mV/s. (c) CV curves of the graphene/CNTs/Mn_2O_3 electrode, prepared by electrodeposition time of 3000s, at scan rates of 10, 20, 30, 40, 50 mV/s, respectively. (d) CV curves of the graphene/CNTs/Mn_2O_3 electrode, prepared by electrodeposition time of 3000s, at scan rates of 1, 2, 5 and 10V/s, respectively. All the CV curves measured in 1.0 M Na_2SO_4 solution.

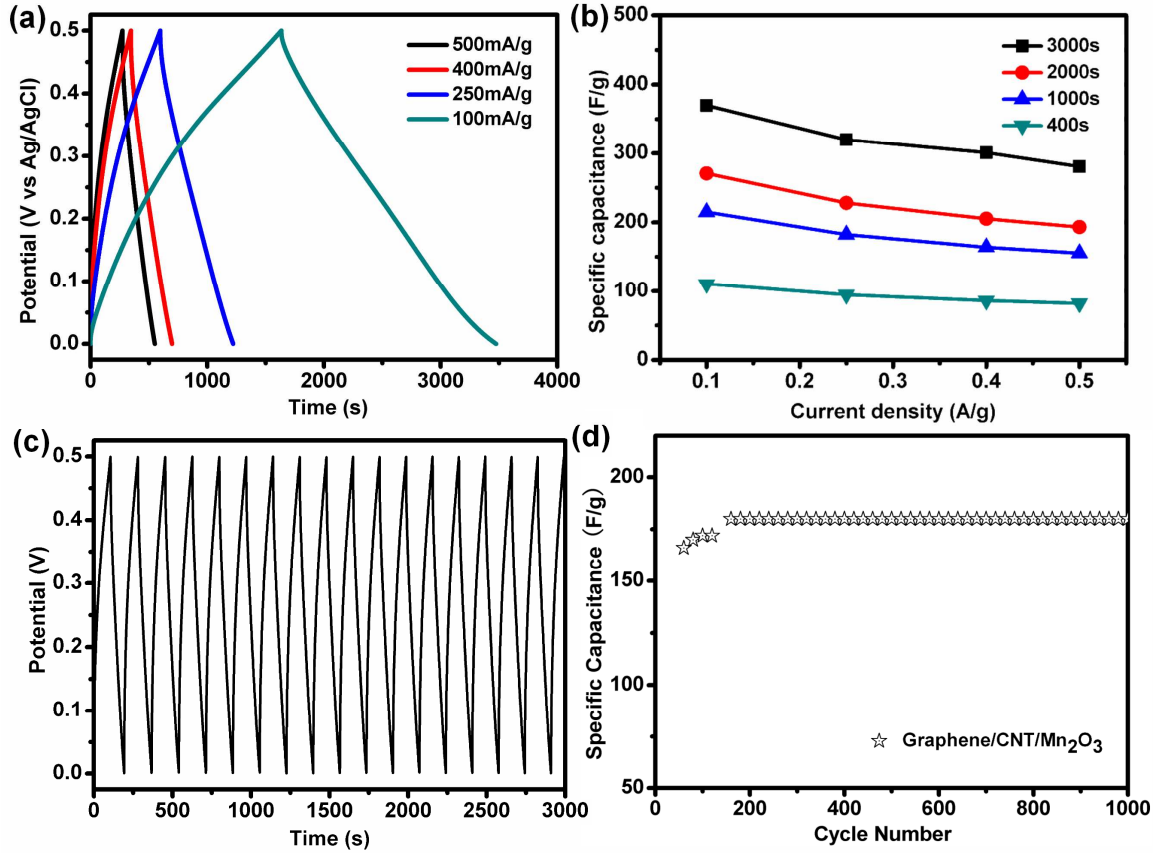

Figure 4. (a) Galvanostatic charge/discharge curves of graphene/CNTs/Mn_2O_3 sandwich electrode, prepared by electrodeposition for 3000s, at different current densities. (b) Effect of electrodeposition time on the specific capacitance of graphene/CNTs/Mn_2O_3 electrode at different current density. (c) Charge/discharge profile of the 3000s deposited graphene/CNTs/Mn_2O_3 electrode at a current density of 1A/g. (d) Evolution of the specific capacitance versus the cycle number at a current density of 1A/g.

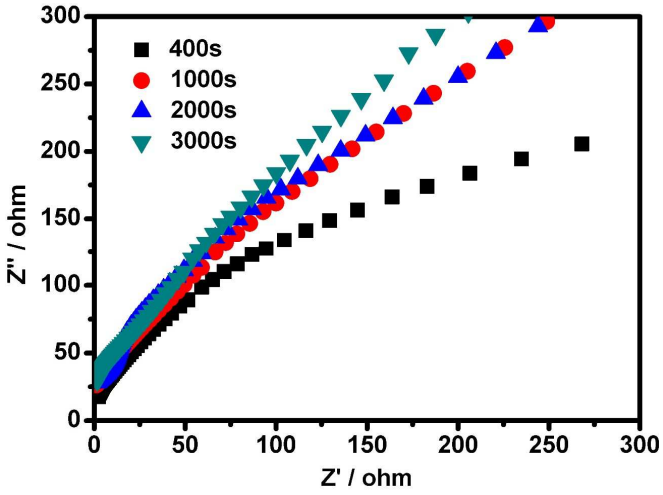

Figure 5. The Nyquist plot of graphene/CNTs/Mn_2O_3 electrodes prepared in 400, 1000, 2000 and 3000 s, respectively.